Diamond & Related Materials 141 (2024) 110642

Contents lists available at ScienceDirect

Diamond & Related Materials

journal homepage: www.elsevier.com/locate/diamond

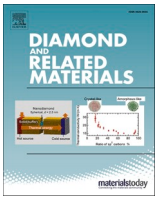

High frequency amplification of acoustic phonons in fluorine-doped single-walled carbon nanotubes

D. Sekyi-Arthur [a,*], S.Y. Mensah [b], E.K. Amewode [b], C. Jebuni-Adanu [c], J. Asare [a]

[a] Department of Physics, School of Physical and Mathematical Sciences, University of Ghana, Legon, Ghana
[b] Department of Physics, College of Agriculture and Natural Sciences, U.C.C, Ghana
[c] Department of Physics Education, University of Education, PMB, Winneba, Ghana

ARTICLE INFO

Keywords:
Carbon nanotube
Fluorine
Cerenkov
Hypersound
Gain

ABSTRACT

Herein, we report on a strong high-frequency induced amplification of coherent acoustic phonons in a non-degenerate fluorine-doped single-walled carbon nanotubes (FSWCNTs) by utilising a tractable analytical approach in the hypersound regime, $ql \gg 1$ (where q is the acoustic wavenumber and l is the carrier mean free path). The acoustoelectric gain obtained is highly nonlinear and is due to stimulated Cerenkov phonon emission by electrically driven carriers undergoing intraminiband transport and capable of performing Bloch oscillations. The transport process causes the carriers to undergo population inversion leading to intraminiband phonon-assisted processes. The generation rate (phonon emission) is expansive and surpasses phonon losses. The threshold field (E_o), at which attenuation switches over to amplification (gain) depends on the FSWCNT parameters (Δ_s&Δ_z), carrier drift velocity ($v_d = \mu E_o$), sound velocity (v_s) and the ratio $\zeta_{s,z}$. This result has potential for intense sources of reasonable acoustic phonons in the sub-THz regime and is vital for the generation of SASER (sound amplification by stimulated emission of acoustic radiation). The amplified phonons also have THz frequencies with wavelengths in the nanometer range, and depends on high spatial parameters which has potential applications for phonon filters and spectrometers.

1. Introduction

Studies of acoustic effects in novel semiconductor by charge carriers has of late attracted much attention [1–4]. Basically, when an acoustic wave goes through a semiconductor, it interacts with several basic excitations. Amid this interactions, the acoustic phonons may lose or pick up momentum and energy in specific situations. The former leads to attenuation while the latter leads to amplification of the acoustic wave [2–4]. The possibility of acoustic wave gain was first observed in CdS [2] and later in n-type Germanium [5,6]. The interaction of acoustic phonons with carriers plays a critical role in the thermal, electronic, optical and thermoelectric properties of semiconductors [5,6]. Extensive work on incoherent phonon generation via hot-carrier relaxation [7,8] has been reported lately by the optical generation of coherent acoustic phonons in bulk and low-dimensional semiconductors [9,10]. Specifically, there are schemes for amplifying acoustic phonons by interaction with co-propagating carriers. Such stable amplification depends on the stimulated emission of acoustic phonons and bosonic elementary excitations upon transitions of the carriers between different carrier states [10].

These studies have generated significant research exercises mostly focussed on two parts of acoustoelectric impact (i.e, ultrasonic enhancement and non-Ohmic conduction) in group II-*VI* and III-V semiconductor compounds such as GaAs, GaSb and InSb [11–13]. Recently, Ref. [14] and Refs. [15, 16] reported on acoustoelectric effect in one-dimensional and two-dimensional structures, respectively. Moreover, the intraminiband absorption of photons by charge carriers in semiconductors is always accompanied by the emission of phonons so that the carriers can gain the necessary momentum for their transitions. The generation and amplification of high frequency phonons have been determined under carrier transport with the carrier velocity surpassing the sound velocity [17], as well as the population inversion of the carrier states [6]. In this situation, amplification is accomplished by utilising any field eg. laser, electric field, carrier concentration or temperature gradient [18] that can cause carrier change.

The Cerenkov emission involves an intraminiband carrier which interacts with co-propagating phonons [19–22]. In bulk materials, the acoustic wave sets up a spatial modulation of the carrier density and

* Corresponding author.
E-mail address: dsekyi-arthur@ug.edu.gh (D. Sekyi-Arthur).

https://doi.org/10.1016/j.diamond.2023.110642
Received 1 February 2023; Received in revised form 9 November 2023; Accepted 16 November 2023
Available online 18 November 2023

trades its energy with that of the carriers by means of deformation potential interaction. Under the influence of an external bias, the fraction of carriers with kinetic energy higher than the phonon energy is upgraded, leading to an improved stimulated emission of acoustic phonons and consequently, a net amplification of the acoustic wave. While this process has been theoretically demonstrated in GHz and THz [20–22] frequency domains, most experimental investigations have stayed restrictedly to phonon frequencies below 100 MHz [22].

Absorption of hypersound in the absence of external electric field in FSWCNT was reported in Ref. [23]. Mensah and co-workers have also reported on the amplification of hypersound in superlattices (SLs) stimulated with an electric field [24]. The study concluded that the observed amplification is due to Cerenkov discharge of phonons by charge carriers whose carrier speed surpasses the speed of sound [24]. In other reports, the effect of high laser intensity on the attenuation coefficient was considered, i.e. no photon absorption by carriers in SLs [6,25,26].

In this manuscript, we demonstrate a novel monochromatic acoustic phonon amplification at the sub-THz frequencies regime. The significance of the source to operate in the monochromatic-mode is to allow it to reach the sub-THz range. The aim of this study is to evaluate a monochromatic acoustic phonon amplification in the sub-THz frequencies regime in FSWCNT as a function of the carrier drift velocity, the acoustic frequency, the carrier-phonon interaction, the carrier concentration, the temperature and the applied electric field. The charge transport mechanism in FSWCNT is deeply influenced by deformation potential interactions. Associated with this deformation potential coupling is a strong acoustoelectric amplification, which can be harnessed for applications in acousto-optic modulators and sound microscopy of high resolutions [27]. However, the different behaviours corresponding to different acoustic wavelengths shows the different length scales over which the acoustic waves interacts with the carrier properties of FSWCNT. To the best of our knowledge, no work has been reported on acoustoelectric amplification in FSWCNT with double periodic band structure.

A “double periodic band structure” typically refers to the electronic band structure of a crystal that exhibits two periodicities. These two periodicities are a result of the crystal lattice structure and the periodicity of the wave functions associated with the electrons.

Crystal Lattice Periodicity: Crystals are composed of repeating units, often referred to as unit cells, that are stacked together in a regular, periodic arrangement. This periodicity in the arrangement of atoms or ions gives rise to a set of allowed energy states for electrons, known as energy bands. These bands have energy gaps between them, which are known as band gaps.

Wave Function Periodicity: Electrons in a crystal are described by wave functions. These wave functions are solutions to the Schrödinger equation for electrons in the periodic potential created by the crystal lattice. The wave functions themselves exhibit periodicity because they are subject to the same periodic potential. This wave function periodicity results in the formation of energy bands. The combination of these two periodicities gives rise to a double periodic band structure. One periodicity is associated with the crystal lattice (the real space periodicity), and the other is associated with the wave functions (the reciprocal space periodicity). The reciprocal space periodicity is often described using the concept of a Brillouin zone. The Brillouin zone is a mathematical construct used to describe the periodicity in reciprocal space. It plays a crucial role in understanding the electronic properties of materials, such as their electrical conductivity and optical properties.

In a nutshell, a double periodic band structure is a characteristic feature of crystalline materials, where two periodicities (one from the crystal lattice and the other from the wave functions) combine to determine the allowed energy states for electrons, leading to the formation of electronic bands and band gaps in the material’s energy spectrum. This structure is essential for understanding the electronic and optical properties of the material.

Theory.

Consider a carrier-phonon system, where the carriers are assumed to be drifting relative to the lattice ions owing to an external electric field. In this process, we ignore carrier-carrier interactions because the wavelength of the phonons is assume to be short compared with the screening length of the carriers. Furthermore, it will only produce higher-order corrections to the phonon distribution function which is assumed to be weak and treated as a perturbation. The problem is solved in the quasi-classical case by making use of the following conditions; (i) $\Delta_{s,z} \gg \tau^{-1} (\hbar = 1)$: This condition implies that the energy gap between the spin-up and spin-down states, denoted by $\Delta_{s,z}$, is larger than the inverse of the scattering time τ. Thus, scattering processes between the spin states are negligible compared to the energy difference. (ii) $\omega \gg 1/\tau$: This condition means that the frequency of the electric field ω should be much larger than the inverse scattering time $1/\tau$, indicating that the system responds quickly to the external field. (iii) $\omega_q \ll \vartheta(p)$: This condition assumes that the characteristic phonon frequency ω_q is much smaller than the energy $\vartheta(p)$ of the carriers. In other words, the energy carried by the carriers dominates over the energy associated with phonons. (iv) $\omega \gg \Delta_{s,z}$: The frequency of the external electric field should be much larger than the energy gap between the spin states. It ensures that the energy provided by the electric field is sufficient to drive transitions between the spin states. (v) Carriers are available only in the lowest miniband, and interminiband transitions are neglected: This assumption implies that the carriers (i.e. electrons or holes) are confined to the lowest energy miniband in the FSWCNT. Transitions between different minibands are disregarded, simplifying the problem by focusing only on the behaviour of carriers within the lowest miniband. (vi) The carrier gas is non-degenerate: This condition suggests that the carrier gas is in a non-degenerate state, meaning that the distribution of carriers follows classical statistics rather than quantum statistics. It allows for the use of classical approaches in analysing the FSWCNT’s carrier behaviour. (vii) The phonons, which represent the lattice vibrations, are in a state of thermal equilibrium. This implies the distribution of phonons follows a thermal distribution corresponding to the temperature of the FSWCNT. (viii) For a frequency range of 100GHz to 3THz and a nanotube of 100 nm at a high temperature $> 50K$ (or 5 meV), low-temperature quantum effects such as Coulomb blockade become irrelevant: Under this condition the frequency range and size of the system, along with the temperature, are such that quantum effects like Coulomb blockade can be ignored. In other words, the classical approximation is valid under these conditions. (ix) Wave phenomena such as reflection and tunneling are negligible in the hypersound regime ($q\ell \gg 1$, and $\omega\tau \gg 1$). In this regime, high frequency acoustic phonons can be treated as particles with energy (and momentum), allowing for a semiclassical treatment. The absence of reflections is explained by approximating the slowly varying potential as a large number of small potentials. The small reflections at each interface interfere destructively, resulting in no net reflection. The carriers (phonons in this case) can then be described semiclassically, following Newton’s laws. (x) If the energy gained by the carrier from the external field is much smaller than the overlapping integral (the energy scale associated with the slowly varying potential, $\Delta_{s,z}$) along the characteristic length ($d_{s,z}$) of the system, and the scattering rate (ν) is small compared to the energy picked up by the carrier from the electric field, then the carrier will oscillate within the first miniband with Bloch frequency ($\omega_B = eEd_{s,z}/\hbar$). The carrier’s energy and group velocity become periodic functions of time. In this scenario, the semiclassical approximation $\left(i.e. \Delta_{s,z} \gg eEd_{s,z}\right)$ is satisfied, allowing for the carrier to be treated semiclassically using classical equations of motion. (xi) Under the semiclassical condition, the carrier wave packet, representing the carrier, is treated as a particle. The uncertainty in the electron’s momentum is assumed to be minimal, making the carrier’s energy sharply defined. Additionally, the uncertainty in the carrier’s position is considered to be minimal compared to the spatial variations of the applied and built-in potentials. The motion of the center of the wave packet is described

by the equation $\hbar k/dt = -\nabla\vartheta = F$, which resembles the classical relation between force and momentum. (xii) The relaxation time (τ) which is the characteristic time it takes for a system to return to its equilibrium state after being perturbed. In doped SWCNTs, the relaxation time is much smaller compared to undoped SWCNTs. This suggests that doped SWCNTs exhibit faster relaxation dynamics. The wavelength of the wave is denoted as $\lambda = 2\pi/q$ ($\ell = 10^{-6}cm$), is much less than the carrier free path length, $\lambda = 10^{-6}cm$ (where λ is the phonon wavelength and q is the phonon wavenumber). In this context, the condition $q\ell \gg 1$ is satisfied which implies that the wave's characteristic length scale is much smaller than the average distance a carrier can travel without scattering.

For doped-SWCNTs (FSWCNTs), the relaxation time τ is far smaller than in undoped SWCNTs. For small τ, $\lambda = v\tau \ll 1$. Thus, $\lambda = 2\pi/q$ which means $\lambda \ll \ell$. Thus, small λ yields large q and the hypersound condition, i.e. $q\ell \gg 1$ is satified. The acoustoelectric gain determined from the expression [28–30].

$$\Gamma = \frac{e\Phi\Lambda^2 q^2\tau}{(2\pi\hbar)^2\rho v_s\omega_q}\sum_p\int_0^\infty [F(p)-F(p+q)]\delta(\vartheta_{p+q}-\vartheta_p-\omega_q)d^2p \quad (1)$$

where Φ is the sound flux density, Λ is the deformation potential constant, ρ is the FSWCNT's density, v_s is the velocity of sound and ω_q is the frequency of the acoustic phonons.

Fig. 1(a) illustrates a one dimensional metallic armchair-SWCNT (n, n) doped with fluorine atoms forming a one-dimensional chain. A nanotube of this nature is equivalent to a band with unit cell as shown in Fig. 1(b), where b is the bond length ($c-c$). The width for the F-(n,n) tube equals N periods with a periodic length of $3b$, and the unit cell containing $N = 4n-2$ carbon atoms, where the atomic numbering in the unit cell of the F-(n, n) nanotube are shown in Fig. 1(c). Doped SWCNTs have qualitatively new physical properties for instance, dispersion laws are qualitatively different for doped and undoped SWCNTs. For an armchair F-(5,5) nanotube, dispersion curves are as shown in Fig. 1(d). In this case, the non-additive dispersion curve at the edge of the Brillouin zone lies on the Fermi surface and the derivative of this curve is zero [31].

As a result, we describe the FSWCNT's additive carrier energy dispersion relation as in Refs. [32–36] using the Huckel matrix approximation for a $p-$ type band with a periodicity of $3b_{s,z}$ given as:

$$\vartheta(p) = \vartheta_o - \Delta_s cos\frac{p_s d_s}{\hbar} - \Delta_z cos\frac{p_z d_z}{\hbar}, \quad (2)$$

where $d_s = \sqrt{3}b_s/2$, $d_z = 3\sqrt{3}b_z/2$, and $b_{s,z}$ is the $c-c$ bond length along the helical and axial directions, respectively. The lowest energy of an outer-shell carrier in an isolated carbon atom is ϑ_o, and the real overlapping integral for leaps along the helical ($\mathscr{S}$) and axial ($\mathscr{Z}$) directions are Δ_s and Δ_z, respectively.

The Boltzmann transport equation (BTE) for carriers interacting with acoustic phonons of frequency (ω_q) and wavenumber (q) in the presence of a high frequency electric field is quoted as:

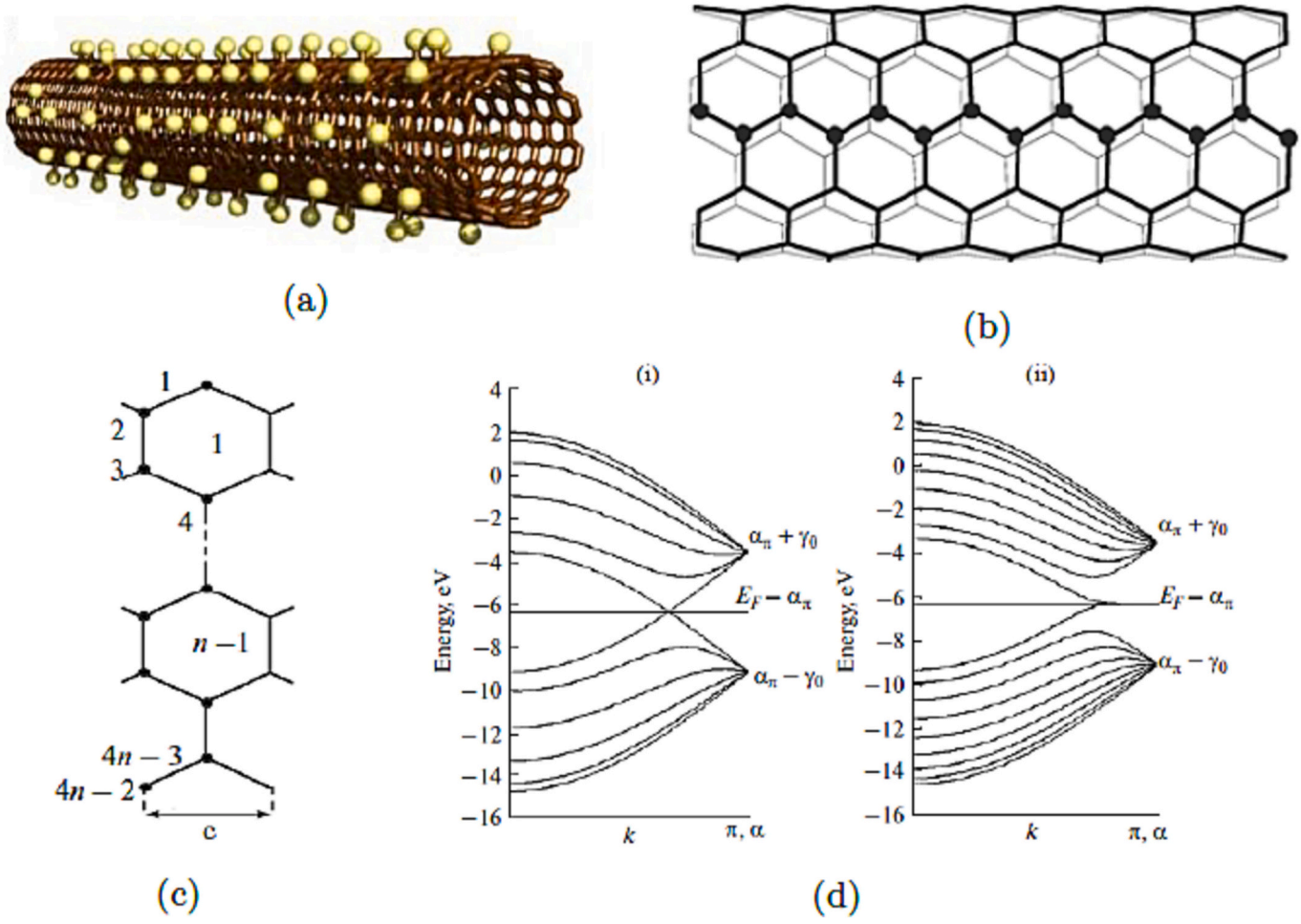

Fig. 1. (a) Fluorine modified SWCNT with the fluorine atoms showing as yellow balls [25], (b) Fluorinated nanotube F $-$ (n,n) (dots denotes the positions of Fluorine atoms of Fluorine atoms that are covalently bonded to C atoms) [30] (c) Atom numbering in the unit cells of nanotubes F $-$ (n,n) [30] (d) $\pi-$ zone of (i) nanotube (5,5) (ii) nanotube F-(5,5), calculated with the parameters, $\alpha_\pi = -6.38$ eV and $\beta_\pi = -2.79$ eV found from benzene spectra [30].

$$\frac{\partial F(p,t)}{\partial t}+e[\mathscr{E}_o+\mathscr{E}_1 cos(\omega t)]\frac{\partial F(p,t)}{\partial p}=-\frac{F(p,t)-F_o(p)}{\tau} \tag{3}$$

where $F(p,t)$ is the non-equilibrium carrier distribution function, $F_o(p)$ is carrier equilibrium distribution function, p is carrier quasi-momentum, and τ is carrier relaxation time. The equation of motion of the FSWCNT carriers under the influence of high-frequency external field with initial condition; $t^{'}=t$, and $p^{'}=p$ is obtained as:

$$\frac{dp^{'}}{dt^{'}}=e[\mathscr{E}_o+\mathscr{E}_1 cos(\omega t^{'})] \tag{4}$$

which has a solution as:

$$p^{'}=e\mathscr{E}_o t^{'}+\frac{e\mathscr{E}_1}{\omega}[sin(\omega t^{'})-sin[\omega(t-t^{'})]] \tag{5}$$

Performing the transformation $p\rightarrow p-p^{'}$, the solution to the BTE, is found by assuming τ to be constant as:

$$F(p,t)=\int_0^{\infty}\frac{dt^{'}}{\tau}exp(-t^{'}/\tau)F_o\left[p-\left(e\mathscr{E}_o t^{'}+\frac{e\mathscr{E}_1}{\omega}[sin(\omega t^{'})-sin[\omega(t-t^{'})]]\right)\right] \tag{6}$$

The equilibrium carrier distribution function is defined by the Fermi-Dirac function:

$$F_o(p)=\frac{1}{1+exp[(\vartheta(p)-\varrho)/T]} \tag{7}$$

where T is the temperature in energy unit, $\mathscr{E}_o$, $\mathscr{E}_1$ and ϱ represents the dc field, ac field and carriers' electrochemical potential, respectively.

When Eqs.(6) and (7) are substituted into Eq. (1), a term $\mathscr{F}_{1/2}$ appears, symbolising the Fermi-Dirac integral of order 1/2 given as [28–30]:

$$\mathscr{F}_{1/2}(\eta_f)=\frac{1}{\Gamma(1/2)}\int_0^{\infty}\frac{\eta_f^{1/2}d\eta}{1+exp(\eta-\eta_f)} \tag{8}$$

where $(\varrho-\vartheta_c)/T\equiv\eta_f$. For a non-degenerate carrier gas, where the Fermi level is several T below the energy of the band edge ϑ_c, i.e. $T\ll\vartheta_c$, the integral in Eq. (8) reduces to:

$$F_o(p)=A^{\dagger}exp\left[\frac{\Delta_s}{T}cos\left(\frac{p_s d_s}{\hbar}\right)+\frac{\Delta_z}{T}cos\left(\frac{p_z d_z}{\hbar}\right)-\left(\frac{\varrho-\vartheta_o}{T}\right)\right] \tag{9}$$

$A^{\dagger}$ is the normalisation constant which is determined using the normalisation condition $n_o=\int_{-\infty}^{\infty}f_o(p)dp$ to be:

$$A^{\dagger}=\frac{n_o d_s d_z}{2I_o(\Delta_s^{*})I_o(\Delta_z^{*})}exp\left(\frac{\varrho-\vartheta_o}{T}\right) \tag{10}$$

where n_o is the carrier concentration, and $I_n(x)$ is a modified Bessel function of order n. Substituting Eqs. (6)–(10) into Eq. (1) yields:

$$\Gamma=\frac{e\Phi\Lambda^2q^2\tau A^{\dagger}}{(2\pi\hbar)^2\rho v_s\omega_q}\sum_p exp\left(\frac{\Delta_z}{T}cos\left(\frac{p_z d_z}{\hbar}\right)\right)$$
$$\times\int_0^{\infty}e^{-t/\tau}\frac{dt^{'}}{\tau}\left[exp\left(\frac{\Delta_s}{T}cos\left(p_s-e\mathscr{E}_o t^{'}-\frac{e\mathscr{E}_1}{\omega}[sin(\omega t^{'})-sin[\omega(t-t^{'})]]\right)d_s\right)\right.$$
$$\left.-exp\left(\frac{\Delta_s}{T}cos\left(p_s+q-e\mathscr{E}_o t^{'}-\frac{e\mathscr{E}_1}{\omega}[sin(\omega t^{'})-sin[\omega(t-t^{'})]]\right)d_s\right)\right]$$
$$\times\delta\left(\frac{\omega_q}{2\Delta_s sin(qd_s/2)}-sin\left(p_s+\frac{q}{2}\right)\right) \tag{11}$$

We invoke a transformation to convert the summation over p into an integral over p within the first Brillouin zone, as follow:

$$\sum_p\rightarrow\frac{2}{(2\pi\hbar)^2}\int_{-\pi/d_s}^{\pi/d_s}dp_s\int_{-\pi/d_z}^{\pi/d_z}dp_z$$

and the acoustoelectric gain takes the form

$$\Gamma=\frac{e\Phi\Lambda^2q^2\tau A^{\dagger}}{(2\pi\hbar)^2\rho v_s\omega_q}\int_{-\pi/d_z}^{\pi/d_z}exp\left(\frac{\Delta_z}{T}cos\left(\frac{p_z d_z}{\hbar}\right)\right)dp_z$$
$$\times\int_0^{\infty}e^{-t/\tau}\frac{dt^{'}}{\tau}\left[exp\left(\frac{\Delta_s}{T}cos\left(p_s-e\mathscr{E}_o t^{'}-\frac{e\mathscr{E}_1}{\omega}[sin(\omega t^{'})-sin[\omega(t-t^{'})]]\right)d_s\right)\right.$$
$$\left.-exp\left(\frac{\Delta_s}{T}cos\left(p_s+q-e\mathscr{E}_o t^{'}-\frac{e\mathscr{E}_1}{\omega}[sin(\omega t^{'})-sin[\omega(t-t^{'})]]\right)d_s\right)\right]$$
$$\times\delta\left(\frac{\omega_q}{2\Delta_s sin(qd_s/2)}-sin\left(p_s+\frac{q}{2}\right)\right) \tag{12}$$

Expressing Γ along the base helix ($\mathscr{S}_\Gamma$) and tubular ($\mathscr{Z}_\Gamma$) directions yields:

$$\mathscr{S}_\Gamma=-\frac{e\Phi\Lambda^2q^2\tau A^{\dagger}}{(2\pi\hbar)^2\rho v_s\omega_q}\int_{-\pi/d_z}^{\pi/d_z}exp\left(\frac{\Delta_z}{T}cos\left(\frac{p_z d_z}{\hbar}\right)\right)dp_z$$
$$\times\int_0^{\infty}e^{-t/\tau}\frac{dt^{'}}{\tau}\left[exp\left(\frac{\Delta_s}{T}cos\left(p_s-e\mathscr{E}_o t^{'}-\frac{e\mathscr{E}_1}{\omega}[sin(\omega t^{'})-sin[\omega(t-t^{'})]]\right)d_s\right)\right.$$
$$\left.-exp\left(\frac{\Delta_s}{T}cos\left(p_s+q-e\mathscr{E}_o t^{'}-\frac{e\mathscr{E}_1}{\omega}[sin(\omega t^{'})-sin[\omega(t-t^{'})]]\right)d_s\right)\right]$$
$$\times\delta\left(\frac{\omega_q}{2\Delta_s sin(qd_s/2)}-sin\left(p_s+\frac{q}{2}\right)\right) \tag{13}$$

and

$$\mathscr{Z}_\Gamma=-\frac{e\Phi\Lambda^2q^2\tau A^{\dagger}}{(2\pi\hbar)^2\rho v_s\omega_q}\int_{-\pi/d_s}^{\pi/d_s}exp\left(\frac{\Delta_s}{T}cos\left(\frac{p_s d_s}{\hbar}\right)\right)dp_s$$
$$\times\int_0^{\infty}e^{-t/\tau}\frac{dt^{'}}{\tau}\left[exp\left(\frac{\Delta_z}{T}cos\left(p_z-e\mathscr{E}_o t^{'}-\frac{e\mathscr{E}_1}{\omega}[sin(\omega t^{'})-sin[\omega(t-t^{'})]]\right)d_z\right)\right.$$
$$\left.-exp\left(\frac{\Delta_s}{T}cos\left(p_z+q-e\mathscr{E}_o t^{'}-\frac{e\mathscr{E}_1}{\omega}[sin(\omega t^{'})-sin[\omega(t-t^{'})]]\right)d_z\right)\right]$$
$$\times\delta\left(\frac{\omega_q}{2\Delta_z sin(qd_z/2)}-sin\left(p_z+\frac{q}{2}\right)\right) \tag{14}$$

The carrier momenta within the first and second quadrant of the first Brillouin zone in the presence of the acoustic phonons for the base helix and tubular directions are obtained as

$$p_s^1=\frac{1}{d_s}sin^{-1}\left(\frac{\omega_q}{2\Delta_s sin(qd_s/2)}\right)-\frac{q}{2}\qquad p_s^2=\frac{\pi}{d_s}sin^{-1}\left(\frac{\omega_q}{2\Delta_s sin(qd_s/2)}\right)-\frac{q}{2} \tag{15}$$

$$p_z^1=\frac{1}{d_z}sin^{-1}\left(\frac{\omega_q}{2\Delta_z sin(qd_z/2)}\right)-\frac{q}{2}\qquad p_z^2=\frac{\pi}{d_z}sin^{-1}\left(\frac{\omega_q}{2\Delta_z sin(qd_z/2)}\right)-\frac{q}{2} \tag{16}$$

Substituting Eqs. (15) and (16) into Eqs. (13) and (14) and invoking standard integrals, Γ along the base helix ($\mathscr{S}$) and tubular ($\mathscr{Z}$) yields:

$$\mathscr{S}_\Gamma=-\frac{e\Phi\Lambda^2q^2\tau n_o d_s^2 d_z\theta(1-\alpha_s^2)}{(\pi\hbar)^2\rho v_s\omega_q\cdot\Delta_s sin(qd_s/2)\sqrt{1-\alpha_s^2}I_o(\Delta_s/T)}$$

$$\times \int_0^{\infty} e^{-t'/\tau}\frac{dt'}{\tau}\left[sinh\left(\frac{\Delta_s}{T}sinAcosBsin\left(\frac{qd_s}{2}\right)\right)cosh\left(\frac{\Delta_s}{T}cosAcosBcos\left(\frac{qd_s}{2}\right)\right)\right.$$

$$\left.-\frac{\Delta_s}{T}cosAsinBsin\left(\frac{qd_s}{2}\right)sinh\left(\frac{\Delta_s}{T}cosAcosBcos\left(\frac{qd_s}{2}\right)\right)cosh\left(\frac{\Delta_s}{T}sinAcosBsin\left(\frac{qd_s}{2}\right)\right)\right], \tag{17}$$

and

$$\mathscr{Z}_{\Gamma} = -\frac{e\Phi\Lambda^2q^2\tau n_o d_s d_z^2\theta(1-\alpha_z^2)}{(\pi\hbar)^2\rho v_s\omega_q\cdot\Delta_z sin(qd_z/2)\sqrt{1-\alpha_z^2}I_o(\Delta_z/T)}$$

$$\times \int_0^{\infty} e^{-t'/\tau}\frac{dt'}{\tau}\left[sinh\left(\frac{\Delta_z}{T}sinAcosBsin\left(\frac{qd_z}{2}\right)\right)cosh\left(\frac{\Delta_z}{T}cosAcosBcos\left(\frac{qd_z}{2}\right)\right)\right.$$

$$\left.-\frac{\Delta_z}{T}cosAsinBsin\left(\frac{qd_z}{2}\right)sinh\left(\frac{\Delta_z}{T}cosAcosBcos\left(\frac{qd_z}{2}\right)\right)cosh\left(\frac{\Delta_z}{T}sinAcosBsin\left(\frac{qd_z}{2}\right)\right)\right], \tag{18}$$

where θ and T are the Heaviside step function, and temperature in energy units, respectively. For $T \gg \Delta_s$ and $T \gg \omega_q$;

$$\mathscr{S}_{\Gamma} = -\frac{e\Phi\Lambda^2q^2\tau n_o d_s^2 d_z\theta(1-\alpha_s^2)}{(\pi\hbar)^2\rho v_s\omega_q\cdot\Delta_s sin(qd_s/2)\sqrt{1-\alpha_s^2}I_o(\Delta_s/T)}$$

$$\times \int_0^{\infty} e^{-t/\tau}\frac{dt'}{\tau}\left[\left(\frac{\Delta_s}{T}sinAcosBsin\left(\frac{qd_s}{2}\right)\right)\right.$$

$$\left.-\left(\frac{\Delta_s}{T}\right)^2 cos^2AsinBcosBcos\left(\frac{qd_s}{2}\right)sin\left(\frac{qd_s}{2}\right)\right], \tag{19}$$

and

$$\mathscr{Z}_{\Gamma} = -\frac{e\Phi\Lambda^2q^2\tau n_o d_s d_z^2\theta(1-\alpha_z^2)}{(\pi\hbar)^2\rho v_s\omega_q\cdot\Delta_z sin(qd_z/2)\sqrt{1-\alpha_z^2}I_o(\Delta_z/T)}$$

$$\times \int_0^{\infty} e^{-t/\tau}\frac{dt'}{\tau}\left[\left(\frac{\Delta_z}{T}sinAcosBsin\left(\frac{qd_z}{2}\right)\right)\right.$$

$$\left.-\left(\frac{\Delta_z}{T}\right)^2 cosA^2sinBcosBcos\left(\frac{qd_z}{2}\right)sin\left(\frac{qd_z}{2}\right)\right] \tag{20}$$

where

$$B = e\mathscr{E}_o d_s t' + \frac{e\mathscr{E}_1 d_s}{\omega}[sin(\omega t') - sin[\omega(t-t')]] \tag{21}$$

Substituting Eq. (21) into Eqs. (19) and (20) and solving explictly yields

$$\mathscr{S}_{\Gamma} = \Gamma_{os}\sum_{k=-\infty}^{\infty}\frac{J_k^2(\chi)}{1+(\Omega\tau+k\omega\tau)^2}\left(1-\frac{\Delta_s^2cos^2Asin(qd_s)}{4TsinAsin(qd_s/2)}\right.$$

$$\left.\times\sum_{k=-\infty}^{\infty}\frac{J_k^2(\chi')(2\Omega\tau+k\omega\tau)}{1+(2\Omega\tau+k\omega\tau)^2}\left(\sum_{k=-\infty}^{\infty}\frac{J_k^2(\chi)}{1+(\Omega\tau+k\omega\tau)^2}\right)^{-1}\right) \tag{22}$$

and

$$\mathscr{Z}_{\Gamma} = \Gamma_{oz}\sum_{k=-\infty}^{\infty}\frac{J_k^2(\chi)}{1+(\Omega\tau+k\omega\tau)^2}\left(1-\frac{\Delta_z^2cos^2Asin(qd_z)}{4TsinAsin(qd_z/2)}\right.$$

$$\left.\times\sum_{k=-\infty}^{\infty}\frac{J_k^2(\chi')(2\Omega\tau+k\omega\tau)}{1+(2\Omega\tau+k\omega\tau)^2}\left(\sum_{k=-\infty}^{\infty}\frac{J_k^2(\chi)}{1+(\Omega\tau+k\omega\tau)^2}\right)^{-1}\right) \tag{23}$$

where

$$\Gamma_{os} = -\frac{e\Phi\Lambda^2q^2n_o d_s^2 d_z\theta(1-\alpha_s^2)\Delta_s^2sin(A)}{T(\pi\hbar)^2\rho v_s\omega_q\sqrt{1-\alpha_s^2}I_o\left(\frac{\Delta_s}{T}\right)} \tag{24}$$

$$\Gamma_{oz} = -\frac{e\Phi\Lambda^2q^2n_o d_z^2 d_s\theta(1-\alpha_z^2)\Delta_z^2sin(A)}{T(\pi\hbar)^2\rho v_s\omega_q\sqrt{1-\alpha_z^2}I_o\left(\frac{\Delta_z}{T}\right)}. \tag{25}$$

We express the high frequency acoustoelectric current density into axial and circumferential components without a loss of generality as; $\Gamma_z = \mathscr{Z}_{\Gamma} + \mathscr{S}_{\Gamma}sin\vartheta_h$ and $\Gamma_s = \mathscr{S}_{\Gamma}cos\vartheta_h$, respectively [37]. The axial carrier thermal current density is expressed as

$$\Gamma_z = \Gamma_{oz}\sum_{k=-\infty}^{\infty}\frac{J_k^2(\chi)}{1+(\Omega\tau+k\omega\tau)^2}\left(1-\frac{\Delta_z^2cos^2Asin(qd_z)}{4TsinAsin(qd_z/2)}\right.$$

$$\left.\times\sum_{k=-\infty}^{\infty}\frac{J_k^2(\chi')(2\Omega\tau+k\omega\tau)}{1+(2\Omega\tau+k\omega\tau)^2}\left(\sum_{k=-\infty}^{\infty}\frac{J_k^2(\chi)}{1+(\Omega\tau+k\omega\tau)^2}\right)^{-1}\right)$$

$$+\Gamma_{os}\sum_{k=-\infty}^{\infty}\frac{J_k^2(\chi)}{1+(\Omega\tau+k\omega\tau)^2}\left(1-\frac{\Delta_s^2cos^2Asin(qd_s)}{4TsinAsin(qd_s/2)}\right.$$

$$\left.\times\sum_{k=-\infty}^{\infty}\frac{J_k^2(\chi')(2\Omega\tau+k\omega\tau)}{1+(2\Omega\tau+k\omega\tau)^2}\left(\sum_{k=-\infty}^{\infty}\frac{J_k^2(\chi)}{1+(\Omega\tau+k\omega\tau)^2}\right)^{-1}\right)sin^2\vartheta \tag{26}$$

and

$$\Gamma_s = \Gamma_{os}\sum_{k=-\infty}^{\infty}\frac{J_k^2(\chi)}{1+(\Omega\tau+k\omega\tau)^2}\left(1-\frac{\Delta_s^2cos^2Asin(qd_s)}{4TsinAsin(qd_s/2)}\right.$$

$$\left.\times\sum_{k=-\infty}^{\infty}\frac{J_k^2(\chi')(2\Omega\tau+k\omega\tau)}{1+(2\Omega\tau+k\omega\tau)^2}\left(\sum_{k=-\infty}^{\infty}\frac{J_k^2(\chi)}{1+(\Omega\tau+k\omega\tau)^2}\right)^{-1}\right)cos\vartheta sin\vartheta \tag{27}$$

where $\chi' = 2\chi = 2e\mathscr{E}_1 d_s/\omega$ and $\Omega_o = \Omega = e\mathscr{E}_o d_{s,z}$. Simplifying further yields

$$\Gamma_z = \Gamma_{oz}\sum_{k=-\infty}^{\infty}\frac{J_k^2(\chi)(1-\zeta_z)}{1+(\Omega\tau+k\omega\tau)^2} + \Gamma_{os}\sum_{k=-\infty}^{\infty}\frac{J_k^2(\chi)(1-\zeta_s)sin^2\vartheta}{1+(\Omega\tau+k\omega\tau)^2} \tag{28}$$

and

$$\Gamma_s = \Gamma_{os} \sum_{k=-\infty}^{\infty} \frac{J_k^2(\chi)(1-\zeta_s)cos\vartheta sin\vartheta}{1+(\Omega\tau+k\omega\tau)^2} \tag{29}$$

where

$$\zeta_{s,z} = \frac{\Delta_{s,z}^2 cos^2 A sin\left(qd_{s,z}\right)}{4TsinAsin\left(qd_{s,z}/2\right)} \sum_{k=-\infty}^{\infty} \frac{J_k^2(\chi')(2\Omega\tau+k\omega\tau)}{1+(2\Omega\tau+k\omega\tau)^2} \left(\sum_{k=-\infty}^{\infty} \frac{J_k^2(\chi)}{1+(\Omega\tau+k\omega\tau)^2} \right)^{-1} \tag{30}$$

and $\zeta_{s,z}$ is a dimensionless parameter defined as the ratio of the carrier drift velocity (v_d) to the sound velocity (v_s) in the medium.

2. Results and discussion

A novel idea of monochromatic acoustic phonon amplification in FSWCNT within the THz frequency region has been examined in this formulation. Coherent phonons propagate in the forward and backward directions along the FSWCNT's axis due to impulsive phonon stimulation by a picosecond laser pulse, resulting in a stationary acoustic wave. Phonons are created when an acoustic wave interacts with an electrically driven intraminiband transition carrier current within a carrier miniband. The intravalley or intraminiband character of the carrier transport allows for much higher currents than intervalley or interminiband carrier and thus, a much stronger phonon amplification by >200 % had been reported [5].

The pertubation theory of carrier transition was employed, where the FSWCNT carriers were anticipated to migrate away from the lattice ions. Carrier-carrier and phonon-phonon interactions as well as phonon losses are ignored but the carrier-phonon interactions are considered to be weak and hence treated as a perturbation [28–30,36]. As can be seen from Eq. (28), Γ_z/Γ_{oz} becomes negative whenever $1 < \zeta_{sz}$, corresponding to gain in acoustic phonons (amplification). Hence, the phonon amplification is obtained for a particular band of phonon wavevectors/wavenumbers. This behaviour of the FSWCNT suggests that it can be used as a phonon filter [23]. To provide a physical interpretation to Eq. (28), a numerical approach was adopted to model the metrics using the following parameters: $\omega_q = 100 \times 10^9 s^{-1}$, $v_s = 2.5 \times 10^3 m/s$, $\Phi = 10^5 Wb/m^2$ $\ell = 10^{-4} cm$ and $q = 10^6 cm^{-1}$.

In Fig. 2, the behaviour of Γ_z/Γ_{oz} as a function of the electric field $\Omega\tau$ for different values of acoustic phonon frequencies ω_q, at $T = 300K$ is displayed. It is observed that Γ_z/Γ_{oz} rises steadily to a positive resonance maximum value indicating the attenuation or absorption of acoustic phonons by the carriers before it falls slowly and approaches zero when $\Omega\tau \approx 0$, and then Γ_z/Γ_{oz} becomes more negative until it reaches a resonant minimum. This extreme negative region observed indicates the emission of acoustic phonons and thus, causing amplification of the acoustic phonons. At this juncture, the amplification surpasses attenuation by comparing the peak of the maximum and minimum values of the plotted curves. This is due to a shift in the external dc electric field's sign. The observed behaviour can be attributed to to the fact that, the FSWCNT excited by the picosecond optical pump in the presence of electric bias, generates coherent FSWCNT phonons at sub-THz frequencies, where the phonon wave propagating along with the electric current exchange energy through deformation potential interactions. The ratio of the carrier velocity to the sound velocity along the axial direction becomes greater than one ($1 < \zeta_z$), in the FSWCNT medium. With several carriers assuming such velocity i.e.,$1 < \zeta_s$, population inversion of carriers with the same energy is then induced because of electric momentum displacement. Thus, a phonon with energy $\hbar\omega_q^{in}$ incident on a carrier which has achieved population inversion, causes it to fall into a lower energy state within the same miniband. This transition is indirect in the FSWCNT momentum space, and results in a phonon with energy $\hbar\omega_q^{em}$ being emitted and amplifying the phonon population; and that the transition occurs from an initial state with higher population of carriers (but low phonon population) than that of the final state with lower population of carriers (but higher phonon population). The FSWCNT phonons can then produce a narrow beam of coherent, high frequency 'sound', known as SASER. This behaviour is observed for various values of ω_q.

We numerically computed peak to peak value of each curve plotted as; for $\omega_q = 0.3THz$, $\Gamma_{amp}/\Gamma_{abs} \approx 1.193$, for $\omega_q = 0.5THz$, $\Gamma_{amp}/\Gamma_{abs} \approx 1.225$, for $\omega_q = 0.7THz$, $\Gamma_{amp}/\Gamma_{abs} \approx 1.259$ and for $\omega_q = 0.9THz$, $\Gamma_{amp}/\Gamma_{abs} \approx 1.294$. It is inferred that when carriers' kinetic energy is greater than that of the sound wave, this leads to the condition $1 < \zeta_s$ and thus, the carriers transfers their energy and momentum to the acoustic waves, leading to the amplification (gain) of acoustic phonons. Moreover, when the carrier's kinetic energy is less than or equal to the velocity of sound in the medium, the acoustic waves pass the energy and momentum to the carriers leading to attenuation (absorption) of acoustic phonons.

Under external bias, increasing the acoustic frequency (ω_q) increases the phonons kinetic energy and carrier drift velocity and more carriers perform intraminiband transition to interact with the phonons. Increasing the external bias further increases $1 < \zeta_s$ in the FSWCNT, which leads to the condition; $1 < \zeta_s$. In otherwords, under the external bias, the fraction of carriers with kinetic energy higher than the phonon

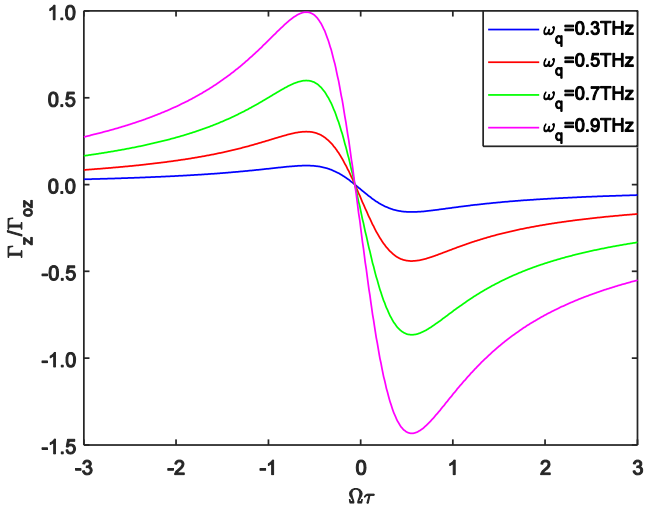

Fig. 2. Dependence of Γ_z/Γ_{oz} on $\Omega\tau$ for varied frequencies ω_q at $T = 300K$.

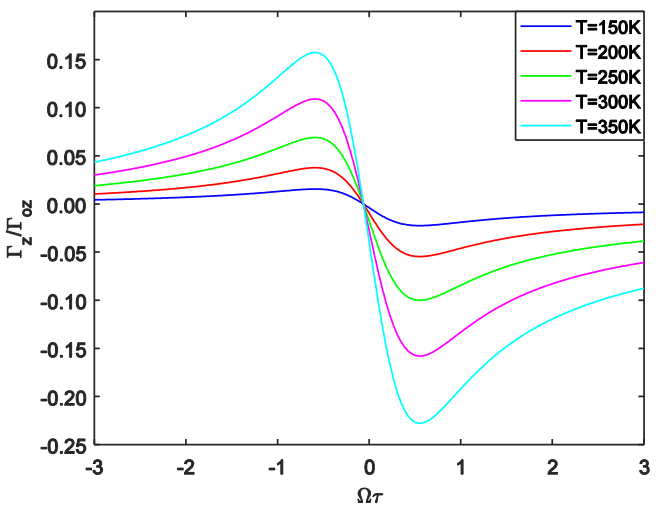

Fig. 3. Dependence of Γ_z/Γ_{oz} on $\Omega\tau$ for varied temperature$T$.

energy is enhanced, which result in an enhanced stimulated emission of acoustic phonons and thus, a net amplification of the acoustic wave. The amplification occurs when carriers transfer energy and momentum to the acoustic waves in excess of their Ohmic losses [38]. The transfer of energy and momentum can also be reflected in a change in the transport characteristics of the carriers. For instance, under the appropriate conditions, the growth of intrinsic acoustic flux via the deformation interaction can be intense enough to lead to strong electrical nonlinearities, which are associated with the formation of acoustoelectric domains with accompanying oscillations in the current [38].

Increasing temperature increases Γ_z/Γ_{oz} dependence on $\Omega\tau$ for different values of temperature (see Fig. 3) owing to the decrease in scattering processes along the axial direction of the FSWCNT. The product of carrier (i.e. electron and hole) concentrations in the FSWCNT under thermodynamic conditions is given as

$$p^{+}n^{-} = N_c exp\left(-\frac{\vartheta_c - \vartheta_F}{kT}\right)\cdot N_v exp\left(-\frac{\vartheta_F - \vartheta_v}{kT}\right) = N_c N_v exp\left(-\frac{\vartheta_g}{kT}\right) \quad (31)$$

where p^{+}, n^{-}, N_c, N_v, ϑ_c, ϑ_v, ϑ_F and ϑ_g are the hole concentration, electron concentration, conduction band, valence band, Fermi energy and the band gap respectively. From Eq. (31), when the temperature is raised an increasing number of carriers gather sufficient thermal energy to leave the FSWCNT atoms and become free to move in the crystal. These carriers are called "free carriers". Since they can move in the crystal they can contribute to an electrical conductivity. The conductivity of a material directly depends on the number of free carriers it contains (free electrons and holes), and the larger the number of carriers, the higher the conductivity. Thus, the conductivity of the FSWCNT increases with temperature (see Fig. 3). The introduction of Fluorine (F) as an acceptor atom in the SWCNT gives rise to a permitted energy level in the bandgap. This level is located a few meV above the top of the valence band. At room temperature electrons in the top of the valence band possess enough thermal energy ($\approx kT/e = 25.6meV$) to "jump" into the energy levels created by the impurity atoms (or: valence electrons are "captured" by acceptor atoms), which gives rise to holes in the valence band. These holes are free to move in the crystal. When an electron is captured by an acceptor atom, a hole is thus released in the crystal, and the acceptor atom (fluorine) becomes ionised (F^{-}) and carries a negative charge, $-e$. Due to the high electron concentration of the SWCNT, more electrons are captured by the impurity atom (F), resulting in the release of more holes in the crystal resulting in high conductivity. This energetic carriers (holes) which are the majority perform intraminiband transition which allows them to achieve population inversion. Thus, it is the intraminiband carrier current generated that interacts with the acoustic phonons leading to an increase in stimulated emission of phonons.

The dependence of Γ_z/Γ_{oz} on $\Omega\tau$ for fixed values of Δ_z and varying Δ_s and vice versa are presented in Fig. 4. The gain in hypersound surpasses attenuation for various values of Δ_s when Δ_z is fixed (see Fig. 4a). A plot of Γ_z/Γ_{oz} against $\Omega\tau$ for different values of Δ_s increases the gain strongly to about 1.5-folds in comparison with the attenuation. Keeping Δ_s fixed and varying Δ_z results in no change in both attenuation and amplification (see Fig. 4b). Thus, increasing Δ_s gives rise to strong coupling between the carriers and phonons and thus, results in strong attenuation as well as gain. The gain however surpasses attenuation for different values of Δ_s where the ratio $\Gamma_{amp}(\omega)/\Gamma_{abs}$ is about $\approx 2-$ folds in comparison to the attenuation coefficient at room temperature $(T = 300K)$. However, the gain is found to be very high for low Δ_s values as shown in (see Fig. 4a). This behaviour suggests that at low Δ_s, the scattering of carriers decreases and thus, more carriers perform intraminiband transition to interact with the co-propagating acoustic phonons which generate a high acoustoelectric gain.

Moreover, the Cerenkov emission requires the carrier velocity to surpass sound velocity, if the propagation of sound is along the z-axis. An electric momentum displacement causes a population inversion of the acoustic phonons. However, when the kinetic energy of the carriers

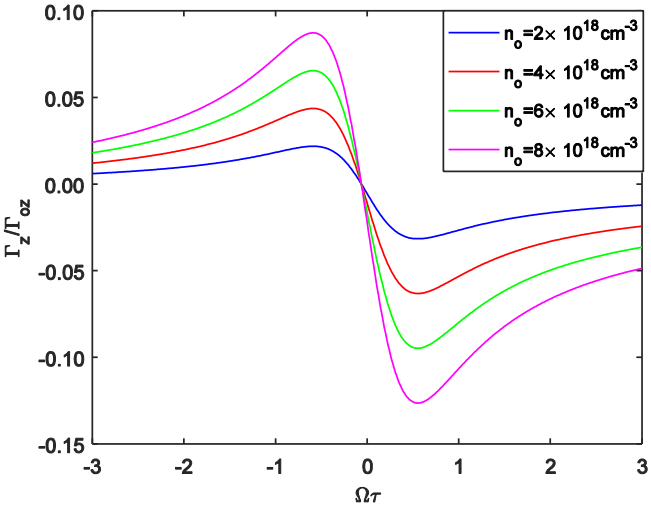

Fig. 5. Dependence of Γ_z/Γ_{oz} on $\Omega\tau$ for varied carrier concentration n_o at $T = 300K$.

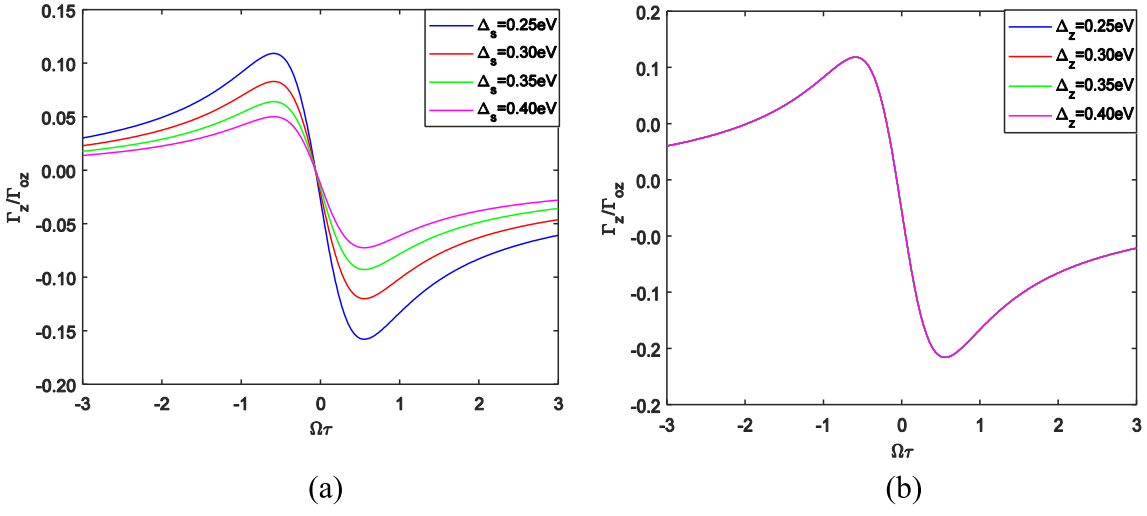

Fig. 4. Dependence of Γ_z/Γ_{oz} on $\Omega\tau$ for $T = 300$ K at (a) varying Δ_s with Δ_z=0.25 eV and (b) varying Δ_z with Δ_s=0.25 eV.

is equal to or less than the kinetic energy of the acoustic wave, the net amplification of the acoustic wave is reduced. As a result, the single carrier dynamics are substantially influenced by the sound wave amplitude. Furthermore, different types of carrier oscillations have been known to be associated with different dynamical regimes, with THz frequencies significantly beyond the GHz frequency of sound waves. The foregoing findings emphasize the importance of events related with carrier interactions with high-frequency phonons. Such results obtained have opened up new avenues for studying carrier dynamics in FSWCNTs in particular.

Fig. 5 shows that Γ_z/Γ_{oz} is sensitive to the surface carrier concentration, n_o. Although it is also very sensitive to $\Omega\tau$ as well, Γ_z/Γ_{oz} for FSWCNT works better for moderate n_o within $1-9\times10^{18}cm^{-3}$ for non-degenerate conditions. Higher n_o increases the gain without screening out the piezoelectric field to lower the gain as in a heterostructure interface like AlGaN/GaN [5]. In other words, carrier-carrier interaction is negligible. Piezoelectric potential coupling [20] is weak as a result of the lattice symmetry and screening at high carrier densities. Carriers with kinetic energies higher than the FSWCNT phonon energy enhance the sound amplitude by the stimulated intraminiband discharge of acoustic phonons, which exploit the population inversion between carrieric states in the same miniband. This Cerenkov instrument acts mostly on the acoustic wave moving in the forward direction, i.e. in the same direction as the carriers. In otherwords, the electric predisposition moves the Fermi distribution of carriers to larger $k-$ vectors, presenting an asymmetric carrier distribution in $k-$ space and enabling phonon gain. The nonlinear rise and fall observed from the study is attributed to Bloch oscillations of the carriers which is a consequence of Bragg's reflections at the band edges [32–36].

In the absence of an external field, the dynamics of intraminiband carriers propagating along the FSWCNT are investigated. A deformation potential is generated by a longitudinal coherent acoustic wave which propagates down the FSWCNT, which results in periodic change of the FSWCNT's conduction band edge. The strain wave generated is assume to propagate down the major axis ($z-$ axis) in this analysis. In the semiclassical regime, the potential energy obtained as a result of the strain (S) on the lattice is given as:

$$V_s = \Lambda S \tag{32}$$

The strain, $S(z,t)$, cause by the coherent acoustic wave which propagates along the $z-$ axis of FSWCNT is calculated as:

$$S(z,t) = -S_o sin\left(qz+\omega_q t\right). \tag{33}$$

The maximum strain for the linear dispersion of acoustic wave of frequency $\omega_q = v_s q$ is calculated as:

$$S_o = qD, \tag{34}$$

where S_o is the mechanical displacement amplitude and D is the displacement of the FSWCNT lattice determined from the acoustic wave. The potential energy generated by the acoustic wave is found by putting Eqs.(33) and (34) into Eq.32 yielding;

$$V_s(z,t) = -\mathscr{U} sin\left(qz+\omega_q t\right), \tag{35}$$

where $\mathscr{U} = \Lambda S_o$ is the amplitude of the acoustic wave. The semiclassical motion equations, which are identical to Hamilton's equations, are as follows:

$$v_z = \frac{\partial \mathscr{H}}{\partial p_z} = \frac{3\sqrt{3}b}{2\hbar} sin\left(3ap_z\right) \qquad \frac{dp_z}{dt} = \frac{\partial \mathscr{H}}{\partial z} = q\mathscr{U} cos\left(q(z+z_o)-\omega_q t\right), \tag{36}$$

with the semiclassical Hamiltonian given as: $\mathscr{H}(z,p_z) = \vartheta(p_z) + V(z,t)$. The drift velocity is solved numerically by making use of Eq. (36), and taking $v_z = 0$, and $p_z = 0$ when $t = 0$, to determine the carrier trajectories in the absence of scattering. The drift velocity (v_d) of the intraminiband carriers dependence on the acoustic wavenumber (q) is presented in Fig. 6.

Carrier dynamics for $q = 5\times10^5 cm^{-1}$, with initial values of $z = 0$, and $p_z = 0$ where high frequency oscillations were driven by the acoustic wave.

The carrier trajectory is a regular, nearly sinusoidal oscillations superimposed on a linear gradient v_z, implies that the acoustic wave drags the carrier through the FSWCNT. The carrier motion is examined in the rest frame of the acoustic wave, where the carrier's location, $z'(t) = z(t) - v_s t$, confirms this image. Further changes in the trajectory results in the following:

$$z(t) = v_s t + \frac{\lambda}{4}[1 - cos(\omega_R t)] \tag{37}$$

where ω_R is the frequency for motion to and fro across the crystal potential wells created.

Fig. 7 shows the region $\omega_R \ll 1/\tau$, which indicats that the drift velocity curve is linear, as is the case with a typical Ohmic current-voltage relationship. The carriers are scattered in this domain before they can be permitted to travel far down the dispersion curve, and the FSWCNT behaves as a pure conductor. In other words, the carriers can only access the lower, parabolic part of the dispersion curve before scattering. As a result, no Bloch oscillation occurs in the region, and Ohmic behaviour is observed. When $\omega_R = 1/\tau$ and the intraminiband carriers' drift velocity

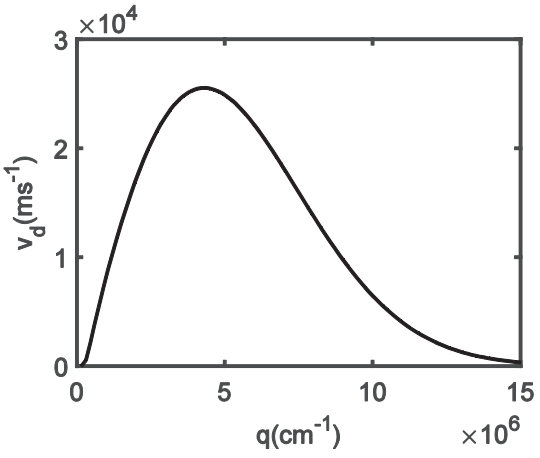

Fig. 6. Carrier dynamics for $q = 5\times10^5 cm^{-1}$, with initial values of $z = 0$, and $p_z = 0$ where high frequency oscillations were driven by the acoustic wave.

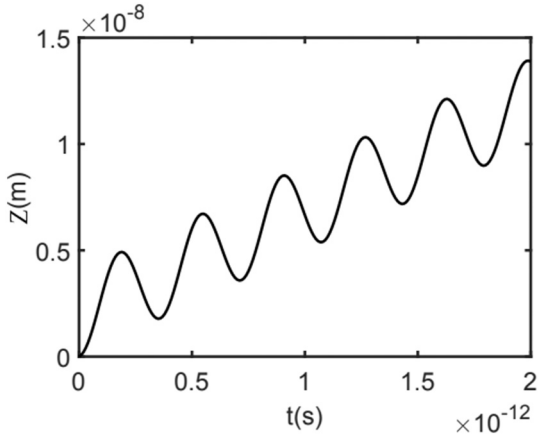

Fig. 7. Carrier dynamics in real space for $q = 4\times10^5 cm^{-1}$, with initial values of $z = 0$, and $p_z = 0$, where the carrier is dragged in the FSWCNT with the velocity of the acoustic wave.

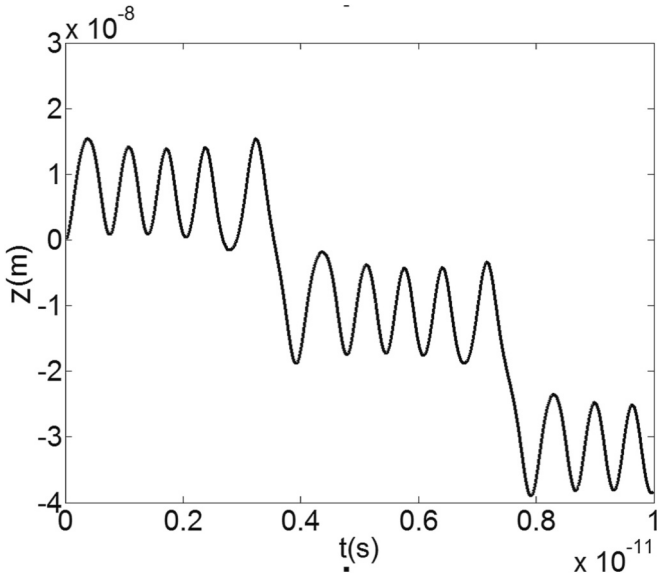

Fig. 8. Carrier dynamics for $q = 5 \times 10^5 cm^{-1}$, with initial values of $z = 0$, and $p_z = 0$ where high frequency Bloch oscillations are driven by acoustic wave.

is at its peak, the carriers are allowed to cross about 0.8 of the Brillouin zone before being scattered.

Carrier dynamics in real space for $q = 4 \times 10^5 cm^{-1}$, with initial values of $z = 0$, and $p_z = 0$, where the carrier is dragged in the FSWCNT with the velocity of the acoustic wave.

Fig. 8 also shows the region $\omega_R > 1/\tau$, which indicates that carriers are suppressed as the field increases, also known as the negative differential conductivity zone. More carriers are permitted to reach the Brillouin zone boundary, and Bloch oscillates before scattering in this region. Bloch oscillations causes the carriers to be confined, which suppresses transport. Furthermore, when the field increases, the carrier's odd of executing a single to numerous Bloch oscillations increases, and the localising effect of these oscillations becomes stronger and stronger, and results in negative differential velocity (NDV). Intraminiband conduction carriers experiences collective high frequency oscillations with frequencies ranging from GHz or sub-THz to THz when NDV is present.

3. Conclusion

Theoretical investigation of strong amplification of coherent acoustic phonons in a non-degenerate FSWCNT utilising the BTE was carried out in the hypersound regime. The acoustoelectric gain obtained is highly nonlinear and was attributed to stimulated Cerenkov phonon emission by electrically driven carriers undergoing intraminiband transport and capable of performing Bloch oscillations. This result has potential application for the development of intense sources of acoustic phonons in sub-THz frequency regime and is vital for generation of SASER. The amplified phonons also have THz frequencies with wavelengths in the nanometer range. Such phenomenon that takes into account examinations with high spatial determination has potential applications in phonon filters, spectroscopy (phonon spectrometer), microbiology, micro-nano carrieric gadgets, tetrahertz adjustment of light, nondestructive testing of microstructures and acoustic examination at room temperatures.

CRediT authorship contribution statement

Conception and design of study: D. Sekyi-Arthur;
Acquisition of data: E.K. Amewode, J. Asare, C. Jebuni-Adanu;
Analysis and/or interpretation of data: S. Y. Mensah, D. Sekyi-Arthur.
Drafting the manuscript: D. Sekyi-Arthur;
Revising the manuscript critically for important intellectual content: D. Sekyi-Arthur, S. Y. Mensah.
Approval of the version of the manuscript to be published: D. Sekyi-Arthur, S.Y. Mensah, E.K. Amewode, J. Asare, C. Jebuni-Adanu.

Declaration of competing interest

The authors declare that they have no known competing financial interests or personal relationships that could have appeared to influence the work reported in this paper.

Data availability

The data that supports the findings of this study are available within the article.

References

[1] B.A. Glavin, V.A. Kochelap, T.L. Linnik, K.W. Kim, M.A. Stroscio, Generation of high-frequency coherent acoustic phonons in superlattices under hopping transport. II. Steady-state phonon population and electric current in generation regime, Phys. Rev. B 65 (8) (2002), 085304.
[2] J. Kent, R.N. Kini, N.M. Stanton, M. Henini, B.A. Glavin, V.A. Kochelap, T.L. Linnik, Acoustic phonon emission from a weakly coupled superlattice under vertical electron transport: observation of phonon resonance, Phys. Rev. Lett. 96 (21) (2006), 215504.
[3] S.Y. Mensah, F.K.A. Allotey, S.K. Adjepong, Acoustoelectric effect in a semiconductor superlattice, J. Phys. Condens. Matter 6 (34) (1994) 6783.
[4] R.P. Beardsley, A.V. Akimov, M. Henini, A.J. Kent, Coherent terahertz sound amplification and spectral line narrowing in a stark ladder Superlattice, Phys. Rev. Lett. 104 (2010), 085501.
[5] Keisuke Shinokita, Klaus Reimann, Michael Woerner, Thomas Elsaesser, Rudolf Hey, Christos Flytzanis, Strong amplification of coherent acoustic phonons by intraminiband currents in a semiconductor superlattice, Phys. Rev. Lett. 116 (7) (2016), 075504.
[6] S.Y. Mensah, N.G. Mensah, V.W. Elloh, G.K. Banini, F. Sam, F.K.A. Allotey, Propagation of ultrasonic waves in bulk gallium nitride (GaN) semiconductor in the presence of high-frequency electric field, Physica E 28 (4) (2005) 500–506.
[7] A. Yamamoto, T. Mishina, Y. Masumoto, M. Nakayama, Coherent oscillation of zone-folded phonon modes in Gaas-Alas Superlattices, Phys. Rev. Lett. 73 (1994) 740.
[8] B.K. Ridley, Hot phonons in high-field transport, Semicond. Sci. Technol. 4 (12) (1989) 1142.
[9] A. Bartels, T. Dekorsy, H. Kurz, K. Khler, Coherent zone-folded longitudinal acoustic phonons in semiconductor superlattices: excitation and detection, Phys. Rev. Lett. 82 (1999) 1044.
[10] K. Mizoguchi, M. Hase, S. Nakashima, M. Nakayama, Observation of coherent folded acoustic phonons propagating in a GaAs/AlAs superlattice by two-color pump-probe spectroscopy, Phys. Rev. B 60 (1999) 8262.
[11] A.M. Lindenberg, I. Kang, S.L. Johnson, T. Missalla, P.A. Heimann, Z. Chang, J. Larsson, P.H. Bucksbaum, H.C. Kapteyn, H.A. Padmore, R.W. Lee, J.S. Wark, R. W. Falcone, Time-resolved X-ray diffraction from coherent phonons during a laser-induced phase transition, Phys. Rev. Lett. 84 (2000) 111.
[12] N. Balkan, B.K. Ridley, J.S. Roberts, Current instabilities in GaAs/GaAlAs single and multiple quantum wells, Superlattices and Microstructures 5 (4) (1989) 539–544.
[13] M.T. Greenaway, A.G. Balanov, E. Scholl, T.M. Fromhold, Phys. Rev. B 80 (2009), 205318.
[14] K.A. Dompreh, K.W. Adu, D. Sakyi-Arthur, N.G. Mensah, S.Y. Mensah, A. Twum, M. Amekpewu, Acoustoelectric Current in Graphene Nanoribbon Due to Landau Damping, 2021.
[15] S.M. Komirenko, K.W. Kim, A.A. Demidenko, V.A. Kochelap, M.A. Stroscio, Generation and amplification of sub-THz coherent acoustic phonons under the drift of two-dimensional electrons, Physical Review B 62 (11) (2000) 7459.
[16] S.M. Komirenko, K.W. Kim, A.A. Demidenko, V.A. Kochelap, M.A. Stroscio, Amplification of transverse acoustic phonons in quantum well heterostructures with piezoelectric interaction, J. Appl. Phys. 90 (8) (2001) 3934–3941.
[17] S.Y. Mensah, F.K.A. Allotey, S.K. Adjepong, The effect of a high-frequency electric eld on hypersound amplification in a superlattice, J. Phys. Condens. Matter 6 (19) (1994) 3479.
[18] S.Y. Mensah, F.K.A. Allotey, N.G. Mensah, V.W. Elloh, Amplification of acoustic phonons in a degenerate semiconductor superlattice, Physica E 19 (3) (2003) 257–262.
[19] S.Y. Mensah, F.K.A. Allotey, N.G. Mensah, Nonlinear acoustoelectric effect in a semiconductor superlattice, J. Phys. Condens. Matter 12 (24) (2000) 5225.
[20] M. Bargheer, N. Zhavoronkov, Y. Gritsai, J.C. Woo, D.S. Kim, M. Woerner, T. Elsaesser, Coherent atomic motions in a nanostructure studied by femtosecond x-ray diffraction, Science 306 (2004) 1771.

[21] G.M. Shmelev, S.Y. Mensah, G.I. Tsurkan, Hypersound amplification by a superlattice in a nonquantised electric field, J. Phys. C Solid State Phys. 21 (33) (1988) L1073.
[22] A.O. Govorov, A.V. Kalameitsev, M. Rotter, J.P. Achim Wixforth, K.H. Hoffmann Kotthaus, N. Botkin, Nonlinear acoustoelectric transport in a two-dimensional electron system, Phys. Rev. B 62 (4) (2000) 2659.
[23] D. Sakyi-Arthur, S.Y. Mensah, N.G. Mensah, K.A. Dompreh, R. Edziah, Absorption of acoustic phonons in fluorinated carbon nanotube with non-parabolic, double periodic band. phonons in low dimensional structures, InTech (2018) 129–142, doi.org/10.5772/intechopen.78231.
[24] S.Y. Mensah, F.K.A. Allotey, N.G. Mensah, V.W. Elloh, Laser induced amplification of hypersound in nondegenerate semiconductor superlattices, Superlattices and microstructures 33 (1) (2003) 41–52.
[25] C. Rodrigues, A.L.A. Fonseca, O.A.C. Nunes, Laser-dressed sound absorption coeffcient in superlattice structures, Phys. Status Solidi B 179 (1) (1993) K17–K20.
[26] S.Y. Mensah, F.K. Allotey, S.K. Adjepong, N.G. Mensah, Photo-stimulated attenuation of hypersound in superlattices, Superlattice. Microst. 22 (4) (1997) 453–457.
[27] R.S. Gilmore, Industrial ultrasonic imaging and microscopy, J. Phys. D Appl. Phys. 29 (6) (1996) 1389.
[28] D. Sakyi-Arthur, S.Y. Mensah, K.W. Adu, K.A. Dompreh, R. Edziah, N.G. Mensah, Acoustoelectric effect in fluorinated carbon nanotube in the absence of external electric field, World Journal of Condensed Matter Physics 10 (2020) 1–11, https://doi.org/10.4236/wjcmp.2020. 101001.
[29] D. Sakyi-Arthur, S.Y. Mensah, K.W. Adu, K.A. Dompreh, R. Edziah, N.G. Mensah, C. Jebuni-Adanu, Induced hall-like current by acoustic phonons in semiconductor fluorinated carbon nanotube, World Journal of Condensed Matter Physics 10 (2020) 71–87, https://doi.org/10.4236/wjcmp.2020. 102005.
[30] D. Sakyi-Arthur, S.Y. Mensah, K.W. Adu, K.A. Dompreh, R. Edziah, N.G. Mensah, C. Jebuni-Adanu, Semiconductor fluorinated carbon nanotube as a low voltage current amplier acoustic device, World J. Condens. Matter Phys. 10 (2020) 12–26, https://doi.org/10.4236/wjcmp.2020.101002.
[31] N.R. Sadykov, E. Yu Kocherga, P.N. Dyachkov, Nonlinear current in modified nanotubes with exposure to alternating and constant electric fields, Russ. J. Inorg. Chem. 58 (8) (2013) 951–955.
[32] D. Sakyi-Arthur, S.Y. Mensah, N.G. Mensah, K.W. Adu, K.A. Dompreh, R. Edziah, Tunable power factor in fluorine-doped single-walled carbon nanotubes, J. Appl. Phys. 128 (24) (2020), 244301.
[33] D. Sekyi-Arthur, M. Egblewogbe, S.Y. Mensah, N.G. Mensah, K.W. Adu, K. A. Dompreh, R. Edziah, S. Atarah, Giant thermoelectric figure of merit in fluorine-doped single walled-carbon nanotubes, Phys. E: Low-Dimens. Syst. Nanostructures 142 (2022) 1–10, 115292.
[34] D. Sekyi-Arthur, S.Y. Mensah, K.A. Dompreh, G. Nkrumah-Buandoh, N.G. Mensah, Giant thermoelectric power in fluorine-doped single-walled carbon nanotubes, J. Phys. Chem. Solid 171 (2022), 111020.
[35] D. Sekyi-Arthur, S.Y. Mensah Jebuni-Adanu, E.K. Amewode, Thermal conductivity in fluorine-doped single-walled carbon nanotubes, Materialia 26 (2022) (101613).
[36] D. Sekyi-Arthur, S.Y. Mensah, E.K. Amewode, R. Arthur, R.R. Adams, Acoustoelectric direct current density in fluorine doped single-walled carbon nanotubes due to harmonic mixing of bichromatic fields with commensurate frequencies, Diamond & Related Materials 136 (2023), 109993.
[37] G.Y. Slepyan, S.A. Maksimenko, A. Lakhtakia, O.M. Yevtushenko, A.V. Gusakov, Electronic and electromagnetic properties of nanotubes, Phys. Rev. B 57 (16) (1998) 9485.
[38] S.K. Abdelraheem, D.P. Blyth, N. Balkan, Amplification of ultrasonic waves in bulk GaN and GaAlN/GaN heterostructures, Phys. Stat. Sol. 185 (2) (2001) 247–256 (a) 185, No. 2, 247-256 (2001).